Simulation and experiment on thermal performance of a micro-channel heat pipe under different evaporator temperatures and tilt angles

Guiqiang Li[a, *]
Guiqiang.Li@hull.ac.uk

Thierno M.O. Diallo[a]

Yousef Golizadeh Akhlaghi[a]

Samson Shittu[a]

Xudong Zhao[a]

Xiaoli Ma[a]

Yingfeng Wang (Revised to "Yinfeng Wang")[b, *]
Guiqiang.Li@hull.ac.uk

[a]School of Engineering, University of Hull, United Kingdom

[b]School of Energy Science and Engineering, Nanjing Tech University, China

[*]Corresponding author.

Abstract

For a solar collector with a heat pipe, the tilt angle is an important factor which has a direct impact on the orientation (surface azimuth angle) and affects the amount of solar radiation reaching the surface of the collector. The performance of the microchannel heat pipe (MCHP), as a highly efficient heat transfer device, can be influenced by gravity and two-phase flow pattern. The relationship between the performance of the MCHP and the tilt angles is nonlinear. In this paper, the effect of the evaporator temperature and tilt angle on the thermal performance of the MCHP, especially the temperature distribution along the heat pipe wall and the effective thermal conductivity, will be investigated. An experimental study with different evaporator temperatures and tilt angles is carried out. Additionally, thermal characteristics of the MCHP have been simulated and verified by the experimental results. In addition, the temperature distribution along the MCHP and the effective thermal conductivity for different working conditions have been performed. These results would provide many references for the solar collector with MCHP system design, optimization, and installation.

Keywords: Solar energy; Microchannel heat pipe; Tilt angle; Thermal conductivity; Heat transfer

1 Introduction

Heat pipes are efficient heat transfer devices which can transport the heat over a distance with a small temperature gradient using the principle of the latent heat of vaporisation [1]. With the development of solar energy, the technology of combining the heat pipe with solar collector is widely being used in engineering and industrial applications. For instance, evacuated tube solar thermal collector [2], flat plate solar thermal collector [3] and Photovoltaic/thermal solar collector [4] can all integrated with the heat pipe. The MCHP can transfer the collected solar thermal energy from its evaporation end to the condensation end in order to produce hot water or hot air.

Currently, the flat plate microchannel heat pipe (MCHP) is one of the most preferred heat pipes since it presents a greater heat transfer characteristics and better performance over the small temperature gradients owing to its micro-channel structure [5,6]. In addition, because of its flat-panel structure, which effectively combines with solar energy, it has gained the attention of the researchers. Deng et al. proposed a novel flat plate MCHP solar collector which produced excellent thermal performance during the experiments [7,8]. Hou et al. also studied a novel photovoltaic-thermal MCHP collector based on the experiment and simulation [9]. Li et al. presented a novel MCHP evacuated tube solar collector for the power and hot water generation [10]. Zhu et al. designed a flat-plate MCHP solar air collector [11]. Zhu et al. investigated the significance of using a MCHP heat exchanger for heat recovery in

residential buildings [12].

For a solar collector with a heat pipe, the tilt angle is an important factor which with a direct impact on the orientation (surface azimuth angle), affects the amount of solar radiation reaching the surface of the collector [13]. Solar collectors need to be tilted at the correct angle to maximize the performance of the system [14]. Mark Z. Jacobson and Vijaysinh Jadhav estimated the optimal tilt angles of PV systems for different cities [15]. Tang and Wu optimized the tile angle of solar collector in China [16]. Huseyin Gunerhan and Arif Hepbasli indicated the optimum tilt angle of solar collectors for building applications [17].

In the solar collector with heat pipe, in addition to the solar radiation, the tilt angle also significantly affects the heat transfer performance of the heat pipe, and consequently the thermal performance of solar collector. Therefore, studying the performance of the MCHP with different tilt angles is necessary for real applications. Deng et al., by an experimental research, investigated the heat transfer characteristics of a MCHP in the flat plate solar collector and showed that when the tilt angle of the MCHP is larger than 30°, the slope change has a negligible effect on the heat transfer performance of flat plate solar collector using a micro heat pipe array [18]. Chen et al. [15] found that the tilt angle of a MCHP influences the thermal performance by experimentally investigating a novel low concentration photovoltaic/thermal system comprising of a MCHP array. They also found that the thermal efficiency increases initially until 65° and then declines as the tilt angle further increases. It is mentioned that when the tilt angle increases, owing to the gravitational force, the recirculation of the working fluid in the condenser increases. However, as the tilt angle increases further, the two-phase flow affects the thermal performance of the system which decreases nonlinearly with tile angle. MCHPs with different structures have different characteristics, and the impact of tilt angle varies according to the structure of the MCHP. In practical applications, the evaporator temperature and tilt angle are the key factors on the performance of the MCHP. Therefore, studying the performance of the MCHP with different evaporator temperatures and under different tilt angles will be an intuitive and efficient way in the improvement of the solar collector installations for reaching the maximize output. However, to the best of our knowledge, no research has been done to systematically evaluate the performance of this type of MCHP with different tilt angles using different evaporator temperatures. So also, this paper has focused on the effect of evaporator temperature of a MCHP for solar collector application.

In this study, the experimental research with different evaporator temperatures and different tilt angles is performed and then the results of both simulation and experimental models with different tilt angles are compared to verify the models. In addition, the predictions of the temperature distribution along the heat pipe with different tilt angles and different evaporation temperatures have also been provided. The current analysis on the effect of the tilt angle would provide a valuable reference for studying, optimization and implementation of the solar collectors with MCHP.

2 Description of a MCHP

The current aluminium flat micro-channel heat pipe contains ten microchannel ports connected in parallel and each microchannel port has micro-fins to enhance the heat transfer rate [19–21] (Fig. 1 (a)). The working fluid evaporates from the evaporator side and moves towards the condenser side along the axis owing to the pressure gradient generated by the difference in temperature. Furthermore, the working fluid releases the latent heat to the cooling medium at the condenser side by an evaporated fluid. Then the working fluid undergoes a phase change from vapour to liquid state and returns to the evaporator side after releasing the heat (Fig. 1 (b)). The geometry of the system is shown in Fig. 1.

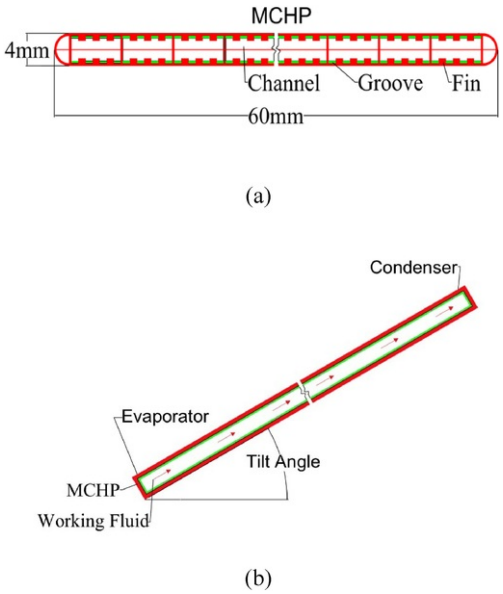

Fig. 1 Schematic diagram of MCHP.

alt-text: Fig. 1

3 Micro-channel heat pipe simulation

In this paper, the mass and heat transfer phenomenon in the micro-channel heat pipe is simulated by ANSYS Fluent 15 software. A two-phase mixture physical model has been built. When the evaporator side is heated, the phase change from the liquid to the vapour occurs during the boiling of the nucleate pool in the evaporator section.

3.1 Model theory

A multiphase model with mixture model has been used. The mixture model can be used to model several phases by solving the mixture equations for momentum, continuity, and energy in addition with the secondary phases volume fraction equations, and the relative velocities algebraic expressions. Furthermore, the Navier-Stokes equations are solved simultaneously in the model. Eqs.(1)–(3) represent the continuity equations which have been used in the simulation of the system,

$$\frac{\partial\left(\rho_m\right)}{\partial t}+\nabla.\left(\rho_m\vec{v}_m\right)=0 \tag{1}$$

where $\vec{v}_m$ is the velocity of the mass-average,

$$\vec{v}_m=\frac{\sum_{k=1}^{n}\alpha_k\rho_k\vec{v}_k}{\rho_m}\vec{v}_m=\frac{\sum_{k=1}^{n}\alpha_k\rho_k\vec{v}_k}{\rho_m} \tag{2}$$

and

$$\rho_m=\sum_{k=1}^{n}\alpha_k\rho_k \tag{3}$$

ρ_m is the density of the mixture, α_k is the phase k volume fraction.

Eq. (4) is the momentum equation which is formed by summing up all the individual momentum equations for all phases.

$$\frac{\partial(\rho_m \vec{v}_m)}{\partial t} + \nabla.\left(\rho_m \vec{v}_m \vec{v}_m\right) = -\nabla \mathrm{p} + \nabla.\left[\mu_m\left(\nabla\vec{v}_m + \nabla\vec{v}_m^T\right)\right] + \rho_m\vec{g} + \vec{F} + \nabla.\left(\sum_{k=1}^{n}\alpha_k\rho_k\vec{v}_{dr,k}\vec{v}_{dr,k}\right) \quad (4)$$

where n is the phases number, $\vec{F}$ is a body force, and μ_m is the viscosity of the mixture: $\mu_m = \sum_{k=1}^{n}\alpha_k\mu_k$. $\vec{v}_{dr,k}$, if the drift velocity for secondary phase k, $\vec{v}_{dr,k} = \vec{v}_k - \vec{v}_m$.

The energy equation is expressed as Eq. (5).

$$\frac{\partial}{\partial t}\sum_{k=1}^{n}\left(\alpha_k\rho_k E_k\right) + \nabla.\sum_{k=1}^{n}\left(\alpha_k\vec{v}_k\left(\rho_k E_k + p\right)\right) = \nabla.\left(k_{eff}\nabla T\right) + S_E \quad (5)$$

where k_{eff} is the effective conductivity, k_t is the turbulent thermal conductivity which is defined according to the turbulence model being used. The first term on the right-hand side of Eq. (5) represents energy transfer due to conduction and s_E includes any other volumetric heat sources. In Eq. (5) the values of E_k has been calculated as:

$$\begin{cases} E_k = h_k - \frac{p}{\rho_k} + \frac{v_k^2}{2}, \ \textit{for a compressible phase} \\ E_k = h_k \ , \textit{for an incompressible phase} \end{cases} \quad (6)$$

where h_k is the sensible enthalpy for phase k .

Equation (7)~(8) is used with the Mixture model for the interphase mass transfer through evaporation-condensation.

The evaporation occurs when $T > T_{sat}$, wherein the mass transfer, $\dot{m}_{1v}$., can be described as

$$\dot{m}_{1v} = 0.1 * \alpha_l\rho_l\frac{\left(T - T_{sat}\right)}{T_{sat}} \quad (7)$$

The condensation occurs when $T < Tsat$, wherein the mass transfer, $\dot{m}_{vl}$, can be described as

$$\dot{m}_{vl} = 0.1 * \alpha_l\rho_l\frac{\left(T - T_{sat}\right)}{T_{sat}} \quad (8)$$

where $\dot{m}_{1v}$ ($\dot{m}_{vl}$) represents the mass transfer rate from the liquid (vapour) phase to the vapour (liquid) phase (kg/s/m^3) and α is the phase volume fraction and ρ is the density. The energy equation source term is obtained by the multiplication of the mass transfer rate and the latent heat.

$$T > T_{sat} \quad S_{E1} = \dot{m}_{e\to v,1lv}\,LH \quad (9)$$

$$T < T_{sat} \quad S_{E1} = \dot{m}_{e\to v,2vl}\,LH \quad (10)$$

where LH is the latent heat vaporisation.

3.2 Geometry and operating conditions of the model

A three-dimensional model was developed to simulate the two-phase heat transfer phenomena in the microchannel heat pipe. The material of the microchannel tube was selected to be aluminium with a total length of 950 mm and a thickness of 0.3 mm. In addition, the condenser and evaporator sections of the MCHP model are 0.1 m in length and the adiabatic section is 0.75 m in length. The heat pipe consists of a microchannel with 10 ports made of aluminium. Each port has six fins, three on the top and three on the bottom. Along the microchannel wall, using seven thermocouples, the temperature distribution was monitored similar to the experimental setup (Fig. 3). The geometry of the model was constructed and meshed with the aid of the ICEM grid generation software. The hybrid/tetrahedral cells have been used for both solid (walls) and fluid zones. The temperature evolution was tested to be independent to the mesh size. Note a total of more than 2,000,000 cells were used in this model. This cell number was limited by the software for present work.

At the inner walls of the microchannel evaporator, boundary condition of non-slip was imposed. Furthermore, at the wall boundaries of the evaporator section, a constant heat flux was defined depending on the power input. While at the adiabatic section and condenser section a boundary condition of zero heat flux was defined (Fig. 2).

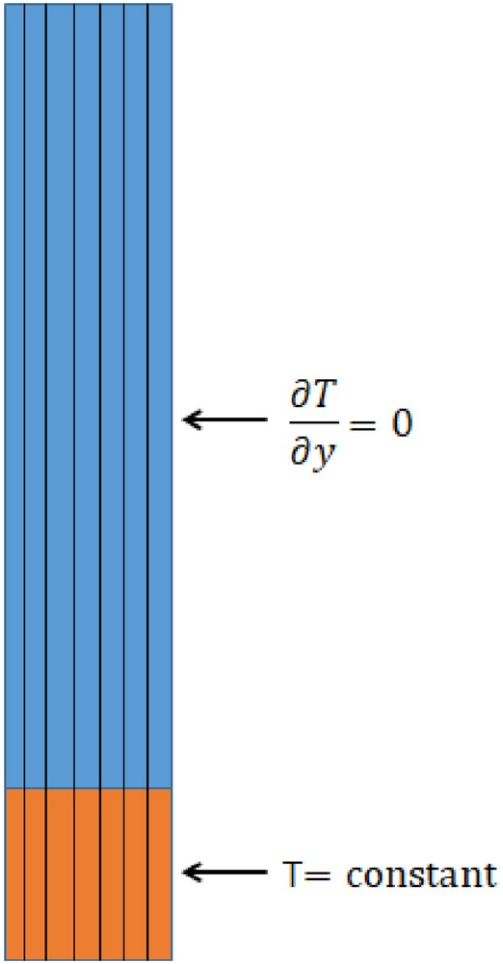

Fig. 2 Boundary conditions (Size: 95 cm*6 cm).

alt-text: Fig. 2

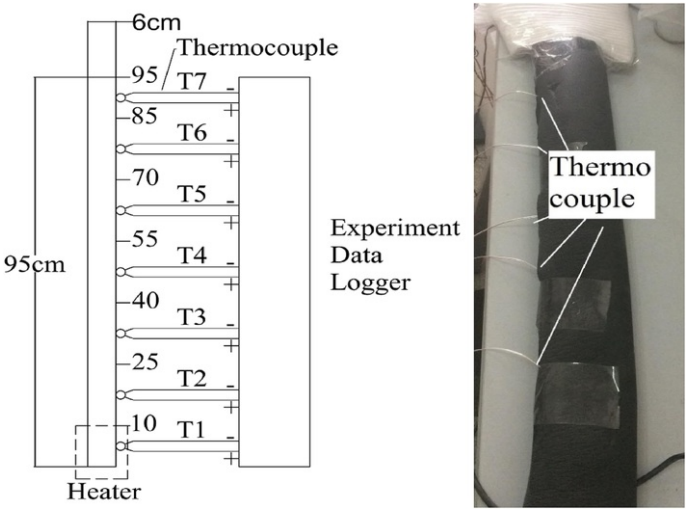

Fig. 3 Test sketch of experiment.

alt-text: Fig. 3

3.3 Model settings

The main settings are presented in Table 1. All the equations are described in the fluent ANSYS user guide [22]. On the completion of filling the pipes with the prescribed amount of working fluid (acetone) under vacuum condition for the greater heat performance and transport, both ends of the MCHP were sealed. The MCHP characterized by a very good performance of heat transfer was enclosed in the insulating materials to reduce thermal losses.

Table 1 Model parameters.

alt-text: Table 1

Model Setting	Parameter	Model Setting	Parameter
Heat pipe wall	Aluminium	Solver	Pressure-based Steady state
Working Fluid Filling ratio	Mixture (acetonevapour/acetoneliquid) 1/3	Viscous	k-e model.
Model	Multiphase model with mixture (evaporation/condensation model)	Solution method	Pressure-velocity coupling (coupled), Momentum, volume fraction and energy discretization (Quick method)

4 Comparison of the simulation and experimental results

4.1 Experiment detail

Seven thermocouples are attached on the surface of the MCHP. The detailed positions of the thermocouples are shown in Fig. 3. The length of the MCHP is 95 cm, and the width of it is 6 cm. The top of the evaporator is enclosed by one heater, and it can provide a stable temperature. The specification of the thermocouple is 0.2 mm copper-constantan, and the experimental relative mean error (RME) is 0.16%, which can be evaluated as below,

$$\mathrm{RME} = \frac{\sum_1^N \frac{\Delta T}{T}}{N} \tag{11}$$

4.2 Comparison and verification

The relative error (RE) between simulation values and experimental results can be calculated by:

$$RE = \frac{X_{exp} - X_{sim}}{X_{exp}} * 100\%. \quad (12)$$

where X_{sim} and X_{exp} are the simulation and experimental values, respectively.

The comparison between the simulated and experimental temperature distribution along the MCHP for different tilt angles (30°, 50°, 70° and 90°) is shown in Fig. 4. The evaporator temperatures at different tilt angles are all about 50 °C. The results of the experiment and simulation are in good agreement, and the maximum deviation among them is 4.1%. In addition, it can be found that the temperature is slightly decreased along the microchannel from the evaporator side to the condenser side, but the temperature decrease varies for different tilt angles, which indicates that the tilt angle affects the heat transfer performance of MCHP.

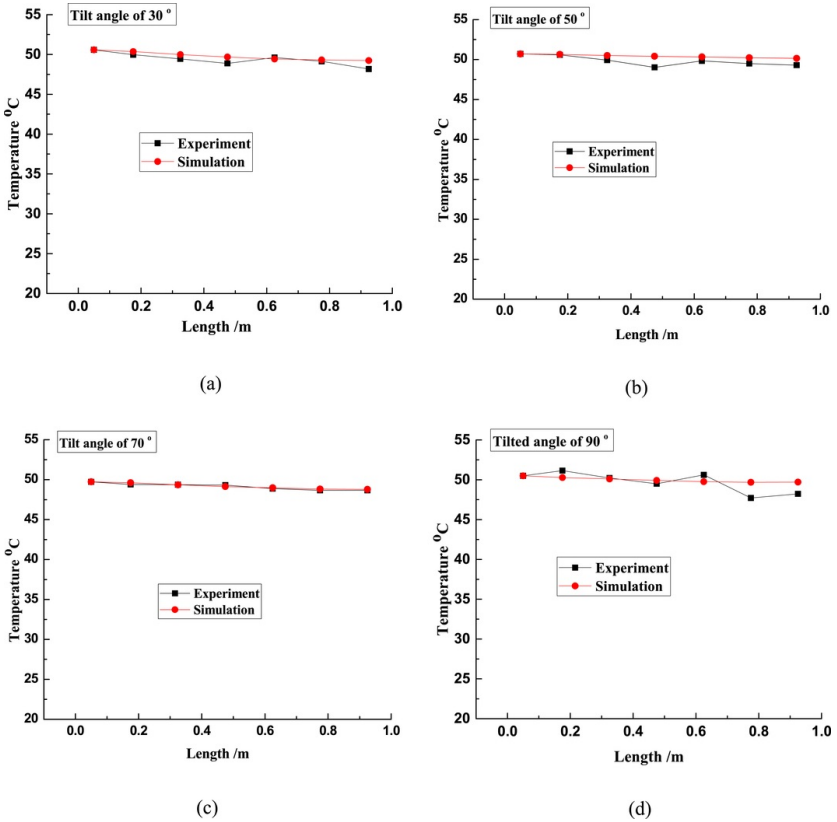

Fig. 4 Wall temperature comparison between simulation and experiment.

alt-text: Fig. 4

5 Performance prediction and analysis

The effect of the angle variation on the micro-channel heat pipe performance has been assessed using the validated computer model. In this paper, the heat pipe performance is characterized by the effective thermal conductivity. The effective thermal conductivity of the microchannel heat pipe, k_{eff}, can be calculated as follows:

$$k_{eff} = \frac{Q_{in} L_{eff}}{A(\Delta T)} \quad (13)$$

where Q_{in} is the heat transfer rate, ΔT is the temperature difference between the evaporator and condenser and L_{eff} is the effective length of the heat pipe. The effective length of the heat pipe is expressed as [23]

$$L_{eff} = \frac{L_e}{2} + L_a + \frac{L_c}{2} \quad \textbf{(14)}$$

where, L_e, L_a, and L_c are the lengths of evaporator, adiabatic and condenser sections of heat pipe.

Fig. 5 presents the evolution of the thermal conductivity according to the evaporator wall temperature (corresponding to different heat inputs) and the angle variation. Firstly, the simulation results show that the tilt angle variation strongly influences the effective thermal conductivity k_{eff}. The thermal conductivity evolution presents different trends and reflects the temperature fluctuation in the micro-channel. Then a horizontal position presents less fluctuation compared to a vertical position. This is due to the fact that as the angle is lower so the gravitational influence is lower and the effective thermal conductivity fluctuation is lower. For lower fluctuations (20° and 30°), k_{eff} tends to increase with the evaporator temperature. Fig. 6 shows the temperature contours in the micro-channel heat pipe when the evaporator temperature is about 50 °C at the tilt angle of 80°. In this temperature condition, the thermal conductivity is higher for an angle of 50° and lower for the angle of 40° (Fig. 5). Higher heat transfer conductivity means a lower thermal gradient in the heat pipe. This behaviour could be explained by the impact of the gravity on the flow pattern according to the tilt angle. The average thermal conductivity shows that the heat pipe is better for a tilt angle of 50°, followed by 70°, 90°, etc.

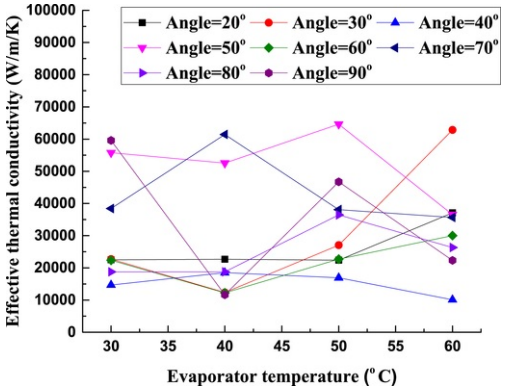

Fig. 5 Influence of evaporator temperature and the tilt angle on the effective thermal conductivity.

alt-text: Fig. 5

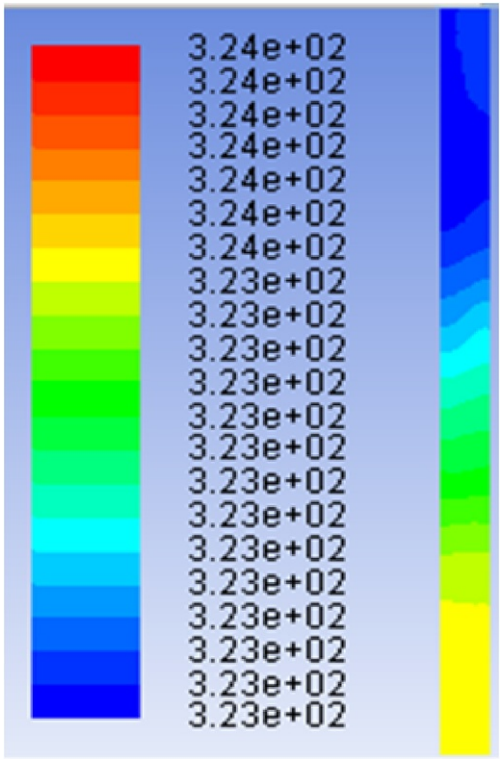

Fig. 6 Contours of the temperature (K) (Size: 95 cm*6 cm).

alt-text: Fig. 6

5.1 Effect of different tilt angles

It can be predicted that with different tilt angles, the temperature differences between evaporator and condenser of MCHP may be different. It is clear that with the low evaporator temperature, the temperature difference shows the obvious fluctuation (Fig. 7). At this evaporator temperature, the temperature difference between the evaporator section and the top of the MCHP indicates a tendency to firstly increase (when the tilt angle <30°), then decrease (30°~60°), and finally increase (60–90°). The temperature difference in the tilt angle range of 50°~70° is much lower than the other tilt angle conditions, indicating the optimal heat transfer performance of the MCHP.

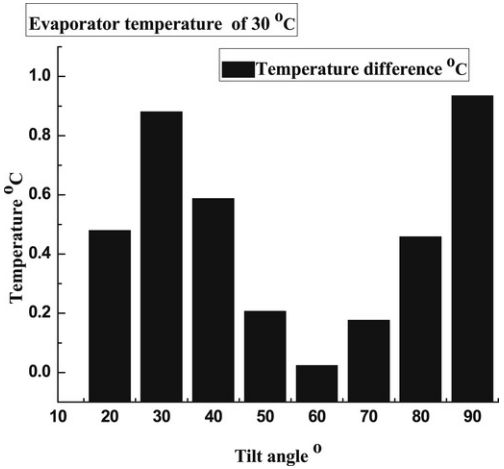

Fig. 7 Temperature difference between evaporator and condenser of MCHP with different tilt angle at the evaporator temperature of 30 °C.

alt-text: Fig. 7

When the evaporator temperature is up to 50 °C and 60 °C, the temperature differences between evaporator and condenser of MCHP shows different tendencies from that with the evaporator temperature of 30 °C (Fig. 8 and Fig. 9). In general, for the high evaporator temperature, the larger tilt angle is corresponding to the high heat transfer performance. It is very complex that the heat transfer performance is dominated by many factors, e.g. the structure of MCHP, working fluid (type and filling ratio, etc.), evaporator temperature, gravitational force, etc. So the temperature difference depends on the combined action of the above factors. As can be seen from these two figures, the minimum temperature difference both occur at the tilt angle of 50°, which represent the best heat transfer performance of the MCHP.

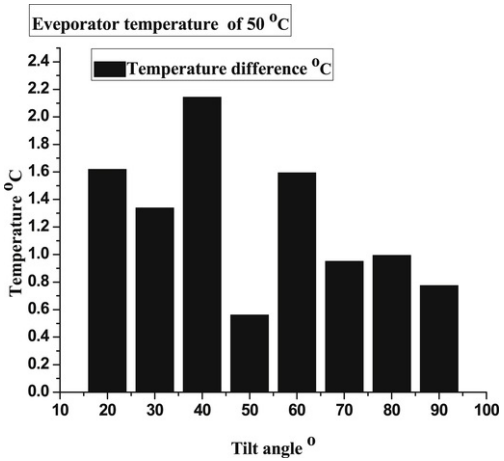

Fig. 8 Temperature difference between evaporator and condenser of MCHP) with different tilt angle at the evaporator temperature of 50 °C.

alt-text: Fig. 8

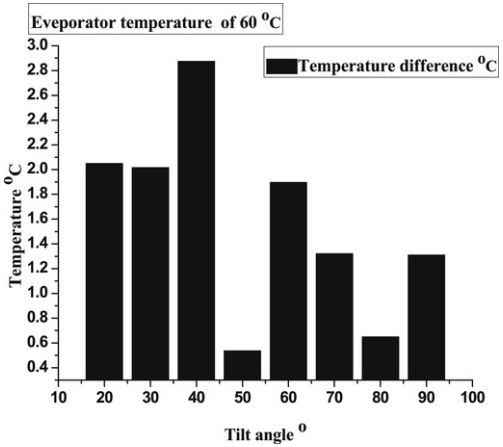

Fig. 9 Temperature difference between evaporator and condenser of MCHP with different tilt angle at the evaporator temperature of 60 °C.

alt-text: Fig. 9

5.2 Effect of different evaporator temperatures

The effect of evaporator temperature was compared and discussed. The results are shown in Figs. 10–12. At the tilt angle of 20°, the different evaporator temperature is corresponding to the different temperature difference between the evaporator and the condenser, as can be seen in Fig. 10. At the same time, it can be observed that with the increase of the evaporator temperature, the temperature difference has an obvious increase tendency.

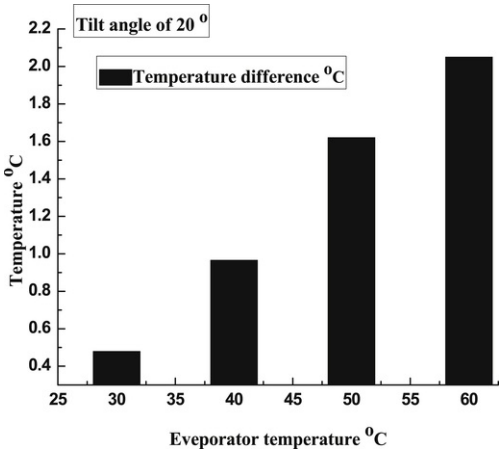

Fig. 10 Temperature difference between evaporator and condenser of MCHP with different evaporator temperature at tilt angle of 20°.

alt-text: Fig. 10

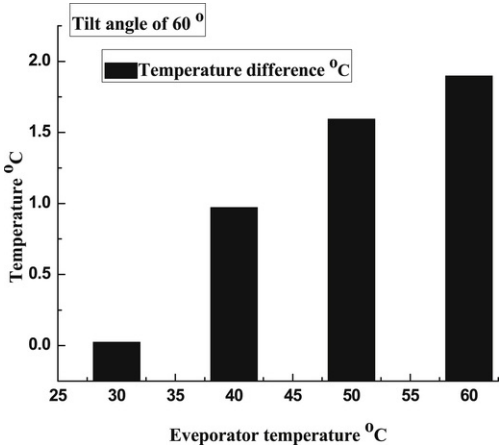

Fig. 11 Temperature difference between evaporator and condenser of MCHP with different evaporator temperature at tilt angle of 60°.

alt-text: Fig. 11

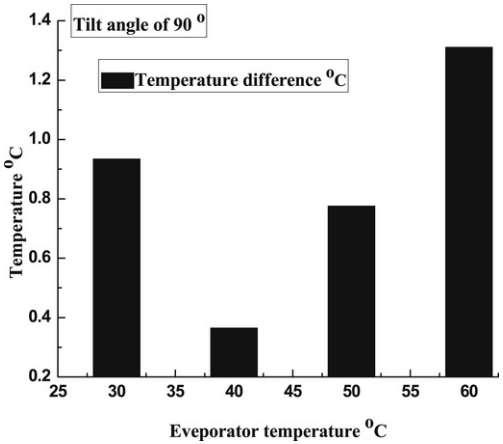

Fig. 12 Temperature difference between evaporator and condenser of MCHP with different evaporator temperature at tilt angle of 90°.

alt-text: Fig. 12

When the tilt angle increases to 60°, the variation tendency of the temperature difference is similar to that of the tilt angle of 20°, and the temperature differences in the whole evaporator temperature range are smaller than that of the tilt angle of 20°. However, the nonlinear trend of temperature difference variation with the different evaporator temperature is more clear when the tilt angle increases.

In addition, when the tilt angle is close to 90°, the variation tendency of temperature difference changes. As can be seen in Fig. 12, the minimum temperature differences occur in the evaporator temperature of 40 °C, i.e. the optimization evaporator temperature is not at the lowest evaporator temperature of 30 °C. That may be because when the tilt angle is 90° if the evaporator temperature is low, the gravitational force of the working fluid would decrease the heat transfer performance.

6 Conclusion

This paper presented an experimental and simulation analyses of the thermal characteristic of a micro channel heat pipe. The simulation of the temperature distribution along the heat pipe and the experiment showed a good agreement. For a MCHP, different evaporator temperatures can match different optimal tilt angles. For example, when the evaporator temperature is about 50 °C, the highest temperature difference was found for a tilt angle was about

40° in most cases. With tilt angle of50°, the temperature gradient was found lower (which means better heat transfer performance for MCHP).

The study also showed that the heat pipe temperature distribution and its effective thermal conductivity depend strongly on the tilt angles with the evaporator temperature. As the tilt angle increases, the temperature fluctuations in the micro-channel increases. This fluctuation is due to the effect of gravity. At the low tilt angle, the temperature difference increases when the evaporator temperature becomes larger, and at the large tilt angle, the change of the temperature difference will be complex with the increase of the evaporator temperature. When the tilt angle increases, the variation of the temperature difference at the different evaporator temperature is also complex, which does not show the obvious tendency, but it can also be seen that the optimization tilt angle is at the middle tilt angles (50°~70°) for different evaporator temperature.

Acknowledgment

The study was sponsored by the Project of EU Marie Curie International Incoming Fellowships Program (745614). The authors would also like to express our appreciation for the financial supports from EPSRC (EP/R004684/1) and Innovate UK (TSB 70507-481546) for the Newton Fund - China-UK Research and Innovation Bridges Competition 2015 Project 'A High Efficiency, Low Cost and Building Integrate-able Solar Photovoltaic/Thermal (PV/T) system for Space Heating, Hot Water and Power Supply' and DongGuan Innovation Research Team Program (No. 2014607101008).

References

[1] G. Li, X. Zhao and J. Ji, Conceptual development of a novel photovoltaic-thermoelectric system and preliminary economic analysis, *Energy Convers Manag* **126**, 2016, 935–943.

[2] Adel A. Eidan, Assaad AlSahlani, Ahmed Qasim Ahmed, Mohamed Al-fahham and Jalal M. Jalil, Improving the performance of heat pipe- experimentally by using Al_2O_3 and CuO/acetone nanofluids, *Sol Energy* **173**, 2018, 780–788.

[3] Lingjiao Wei, Dazhong Yuan, Dawei Tang and Bangxian Wu, A study on a flat-plate type of solar heat collector with an integrated heat pipe, *Sol Energy* **97**, 2013, 19–25.

[4] H. Jouhara, M. Szulgowska-Zgrzywa, M.A. Sayegh, J. Milko, J. Danielewicz, T.K. Nannou and S.P. Lester, The performance of a heat pipe based solar PV/T roof collector and its potential contribution in district heating applications, *Energy* **136**, 2017, 117–125.

[5] G. Li, W. Feng, Y. Jin, X. Chen and J. Ji, Discussion on the solar concentrating thermoelectric generation using micro-channel heat pipe array, *Heat Mass Transf* **53** (11), 2017, 3249–3256.

[6] G. Li, G. Zhang, W. He, J. Ji, S. Lv, X. Chen and H. Chen, Performance analysis on a solar concentrating thermoelectric generator using the micro-channel heat pipe array, *Energy Convers Manag* **112**, 2016, 191–198.

[7] Yuechao Deng, Yaohua Zhao, Wei Wang, ZhenhuaQuan, Lincheng Wang and Dan Yu, Experimental investigation of performance for the novel flat plate solar collector with micro-channel heat pipe array (MHPA-FPC), *App Therm Eng* **54** (2), 2013, 440–449.

[8] Yuechao Deng, Wei Wang, Yaohua Zhao, Liang Yao and Xinyue Wang, Experimental study of the performance for a novel kind of MHPA-FPC solar water heater, *Appl Energy* **112**, 2013, 719–726.

[9] ZhenhuaQuan LongshuHou, Yaohua Zhao, Lincheng Wang and Gang Wang, An experimental and simulative study on a novel photovoltaic-thermal collector with micro heat pipe array (MHPA-PV/T), *Energy Build* **124**, 2016, 60–69.

[10] G. Li, J. Ji, G. Zhang, W. He, X. Chen and H. Chen, Performance analysis on a novel micro-channel heat pipe evacuated tube solar collector incorporated thermoelectric generation, *Int J Energy Res* **40** (15), 2016, 2117–2127.

[11] Tingting Zhu, Yanhua Diao, Yaohua Zhao and Ma Cheng, Performance evaluation of a novel flat-plate solar air collector with micro-heat pipe arrays (MHPA), *Appl Therm Eng* **118**, 2017, 1–16.

[12] Zhong Wei Zhu, Hong Ming Fan and Cheng Zhang, Experimental investigations on the effectiveness of micro heat pipe array heat exchanger for heat recovery for residential building, *Appl Therm Eng* **102**, 2016, 980–988.

[13] Kamal Skeiker, Optimum tilt angle and orientation for solar collectors in Syria, *Energy Convers Manag* **50**, 2009, 2439–2448.

[14] Adnan Shariah, M-Ali Al-Akhras and I.A. Al-Omari, Optimizing the tilt angle of solar collectors, *Renew Energy* **26**, 2002, 587–598.

[15] Mark Z. Jacobson and Vijaysinh Jadhav, World estimates of PV optimal tilt angles and ratios of sunlight incidentupon tilted and tracked PV panels relative to horizontal panels, *Sol Energy* **169**, 2018, 55–66.

[16] Huseyin Gunerhan and Arif Hepbasli, Determination of the optimum tilt angle of solar collectors for building applications, *Build Environ* **42**, 2007, 779–783.

[17] Runsheng Tang and Tong Wu, Optimal tilt-angles for solar collectors used in China, *Appl Energy* **79**, 2004, 239–248.

[18] Xue Z., Qu W. Experimental study on effect of tilt angles to ammonia pulsating heat pipe. Chin J Aeronaut, 27(5): 1122–1127.

[19] Lingen Chen and Huijun Feng, Multi-objective constructal optimizations for fluid flow, heat and mass transfer processes, 2017, Science Press; Beijing.

[20] Huijun Feng, Lingen Chen and Shaojun Xia, Constructal design for disc-shaped heat exchanger with maximum thermal efficiency, *Int J Heat Mass Transf* **130**, 2019, 740–746.

[21] Huijun Feng, Lingen Chen, Zhihui Xie and Fengrui Sun, Constructal entransy dissipation rate minimization of a rectangular body with nonuniform heat generation, *Sci China Technol Sci* **59** (9), 2016, 1352–1359.

[22] ANSYS Fluent, Ansys fluent theory guide: version 13.0, 2010, Ansys Inc.; Canonsburg.

[23] A. Brusly Solomon, M. Sekar and S.H. Yang, Analytical expression for thermal conductivity of heat pipe, *Appl Therm Eng* **100**, 2016, 462–467.

Nomenclature

F: body force [N/m^3]

h: sensible enthalpy [J/kg]

k: effective conductivity [W/m/K]

LH: Latent Heat [J/kg]

m: mass [kg]

p: pressure [Pa]

S: volumetric heat source [W/m^3]

t: time [s]

v: velocity [m/s]

y: dimension [m]

Subscripts

c: condenser

dr: drift

e: evaporator

eff: effective conductivity

k: phase liquid or vapour

l: liquid

m: mixture

n: number of phase sat saturation

t: turbulent

v: vapour

Greek Symbols

ρ : density (kg/m^3)

α : volume fraction [−]

$\vec{v}_m$: velocity [m/s]

μ : dynamic viscosity [Pa.s]

Queries and Answers

Query: Please confirm that the provided email “Guiqiang.Li@hull.ac.uk” is the correct address for official communication, else provide an alternate e-mail address to replace the existing one, because private e-mail addresses should not be used in articles as the address for communication.
Answer: Correct Email address of Yinfeng Wang should be revised to: wangyf@njtech.edu.cn

Query: Please check the author given name and surname.
Answer: The name of this one corresponding author, "Yingfeng Wang", should be revised to "Yinfeng Wang"

Query: Have we correctly interpreted the following funding source(s) and country names you cited in your article: Innovate UK, United Kingdom; EPSRC, United Kingdom?
Answer: Yes

Query: Please confirm that given names and surnames have been identified correctly and are presented in the desired order and please carefully verify the spelling of all authors’ names.
Answer: The given name "Yingfeng" in the author list should be revised to "Yinfeng"

Query: Your article is registered as belonging to the Special Issue/Collection entitled “Energy EU China”. If this is NOT correct and your article is a regular item or belongs to a different Special Issue please contact s.venkiteswaran@elsevier.com immediately prior to returning your corrections.
Answer: Yes